INTERNATIONAL JOURNAL FOR NUMERICAL METHODS IN FLUIDS
Int. J. Numer. Meth. Fluids 2008; **56**:1993–2020
Published online 23 August 2007 in Wiley InterScience (www.interscience.wiley.com). DOI: 10.1002/fld.1580

A general Riemann solver for Euler equations

Hao Wu*,† and Zhijun Shen

Laboratory of Computational Physics, Institute of Applied Physics and Computational Mathematics, Beijing P.O. Box 8009, 100088, People's Republic of China

SUMMARY

In this paper, we present a general Riemann solver which is applied successfully to compute the Euler equations in fluid dynamics with many complex equations of state (EOS). The solver is based on a splitting method introduced by the authors. We add a linear advection term to the Euler equations in the first step, to make the numerical flux between cells easy to compute. The added linear advection term is thrown off in the second step. It does not need an iterative technique and characteristic wave decomposition for computation. This new solver is designed to permit the construction of high-order approximations to obtain high-order Godunov-type schemes. A number of numerical results show its robustness. Copyright © 2007 John Wiley & Sons, Ltd.

Received 9 February 2006; Revised 29 June 2007; Accepted 30 June 2007

KEY WORDS: compressible flow; Euler equations; finite volume method; Godunov-type method; Riemann solvers; complex EOS

1. INTRODUCTION

During the last 30 years, finite volume methods based upon the Riemann problem (RP) have been the dominant computational approach for solving systems of hyperbolic conservation laws. Among them, Godunov [1] and Godunov-type [2] schemes have been particularly efficient in a wide range of scientific disciplines. When Godunov-type methods are applied to more complex physical systems, it is apparent that the main obstacle to this process will be the availability of accurate Riemann solvers, algorithms for solving discontinuous RPs. The Riemann solver, which is the only place in the method where problem-specific information is used, cannot be used generally

*Correspondence to: Hao Wu, Laboratory of Computational Physics, Institute of Applied Physics and Computational Mathematics, Beijing P.O. Box 8009, 100088, People's Republic of China.
†E-mail: wuhao_iapcm@hotmail.com, charmingjason@163.com

Contract/grant sponsor: National Natural Science Foundation of China; contract/grant number: 10431050
Contract/grant sponsor: CAEP; contract/grant number: 2003Z0603
Contract/grant sponsor: LCP; contract/grant number: 51479020105ZW0902

Copyright © 2007 John Wiley & Sons, Ltd.

in different problems. In order to achieve high accuracy, the Riemann solver must be able to sort out wave motions of the specific systems that arise in discontinuous situations.

The exact Riemann solver achieves this by using characteristic wave decomposition analysis, which certainly depends on the form of the governing equations. The problem is that the complexity of such analysis increases rapidly when the governing equations become complex. For sufficiently complex governing equations and equations of state (EOS) in Euler equations, carrying out this task may become extremely difficult, impractical and even impossible. When an exact Riemann solver is applied to the Euler equations of fluid motion, it needs a computationally efficient iterative technique [3]. This question introduces a non-linear set of three coupled equations for the one-dimensional (1-D) case. Solving these equations by an iterative exact method, such as the exact Riemann solver, is not computationally efficient. For perfect gases, exact Riemann solutions for the Euler equations can be found in the literature. However, taking some real gases and some liquids' EOS into account renders the solution of the RP difficult. The solution procedure for real gases and some liquids is similar to that for the perfect gases. However, due to different real-gas models being implemented, the detailed steps can be quite different.

A method to overcome this problem is to use an approximate Riemann solver. There are many approximate solvers in the literature, for example, Roe solver [4, 5], HLL solver [6], HLLC solver [7] and others. As to arbitrary EOS, Buffard *et al.* [8, 9] proposed a universal solver that is independent of the EOS for the Euler equations. HLL and HLLC solvers both show their robustness in simulating the Euler equations for complex EOS. However, in these approximate Riemann solvers, the characteristic wave decomposition or the estimation of Godunov flux is necessary.

Another method uses the central schemes that are not tied to specific details of the governing equations. Here, we just talk about the three-point central schemes. Many such schemes, for example, the Lax–Friedrichs [10] scheme, typically have poor accuracy, because they hardly use the characteristic information. The high-order central schemes, for example, the Lax–Wendroff [11] scheme, are associated with the phenomenon of spurious oscillations in the numerical solution in the vicinity of shocks. For central schemes, it is more difficult than upwind schemes to obtain high accuracy without oscillations because of the lack of physical information.

The Riemann solvers' accuracy and universality seem to be at odds with each other. The best solvable method would feature acceptable accuracy yet not involve extensive characteristic analysis.

In this paper, we aim at exploring a new approach to the design of an accurate, general-purpose Riemann solver algorithm. We will derive an algorithm that is only loosely tied to EOS of the Euler equations and is less dependent on specific characteristic properties of the governing equations. The solver can successfully be applied to compute the Euler equations with many complex EOS. Since the algorithm does not involve characteristic decomposition analysis, it can be used easily in other systems of hyperbolic conservation laws. This makes the new solver an attractive, general-purpose solution method for practical, especially very complex, similar problems. The Riemann solver leads directly, without the need for iteration, to an approximate solution to the RP.

The paper is organized as follows: Section 2 introduces some related background and the new Riemann solver. Several estimates of the linear advection term are compared and a number of test problems are represented in Section 3 to assess the performance of the new Riemann solver in ideal gases. In Section 4, the numerical tests are shown using the Euler equations with a complex EOS. Extension of the solver to two space dimensions is explained briefly in Section 5, and some

Copyright © 2007 John Wiley & Sons, Ltd.

DOI: 10.1002/fld

two-dimensional (2-D) RPs of the Euler equations are shown in this section. Some conclusions can be found in Section 6.

2. THE NEW RIEMANN SOLVER

2.1. Riemann problem

Let us consider an RP for the Euler equations in one dimension. The RP is the initial value problem for a hyperbolic system of conservation laws,

$$\frac{\partial U}{\partial t} + \frac{\partial F(U)}{\partial x} = 0 \tag{1}$$

with initial conditions consisting simply of two constant states separated by a discontinuity

$$U(x, 0) = \begin{cases} U_{\mathrm{L}}, & x < 0 \\ U_{\mathrm{R}}, & x \geqslant 0 \end{cases}$$

where U is $(\rho, \rho u, E)^{\mathrm{T}}$ and $F(U)$ is $(\rho u, \rho u^2 + p, u(E + p))^{\mathrm{T}}$. Here, ρ is the density, u is the velocity, p is the pressure and E is the total energy per unit volume. $E = \frac{1}{2}\rho u^2 + \rho e$, where e is the internal energy.

Suppose A is the Jacobian of the flux function $F(u)$, that is $A(U) = \partial F / \partial U$. The corresponding eigenvalues are $\lambda_1 = u - a$, $\lambda_2 = u$ and $\lambda_3 = u + a$. Here, a is the local sound speed. For each eigenvalue λ_i, $i = 1, 2, 3$, there is a wave family. For the Euler equations, the existence and uniqueness of solution to the RP can only be shown for initial data which are rather close. In fact, related theory is also not perfect. We shall assume that the solution to the RP for the Euler equations exists and only consider convex EOS such that the waves discussed here are shocks, contacts and rarefaction waves. In this paper, van der Waals EOS (as a non-convex EOS) [12] is considered in one phase, which shows that the new solver can simulate Euler equations with a non-convex EOS. The structure of the solution to the RP in the x–t plane is depicted in Figure 1. It consists of four constants and three waves emanating from the origin, one for each eigenvalue λ_i, $i = 1, 2, 3$. The speed of propagation in each family wave is determined by the eigenvalue λ_i. Naturally, the solution to the left of the λ_1 wave is simply the initial data U_{L} and to the right of the λ_3 wave is U_{R}. Now, the task at hand is to find the solution in the wedge between the λ_1 and λ_3 waves.

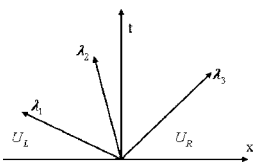

Figure 1. The structure of the solution of the Riemann problem (1).

Copyright © 2007 John Wiley & Sons, Ltd.

DOI: 10.1002/fld

2.2. Godunov method

Godunov scheme is of first-order accuracy as the functions are assumed to be piecewise constants and its modifications that have appeared are for the purpose of increasing the order of accuracy. It is expressed in the following form:

$$U_j^{n+1} = U_j^n - \lambda(F^G(U_j^n, U_{j+1}^n) - F^G(U_{j-1}^n, U_j^n))$$

$$F^G(U_j^n, U_{j+1}^n) = F(V(0; U_j, U_{j+1}))$$

$V(x/t; U_j, U_{j+1})$ is the similarity solution of (1) and the initial value

$$U(x, t_n) = \begin{cases} U_j, & x < x_{j+1/2} \\ U_{j+1}, & x > x_{j+1/2} \end{cases}$$

where $\lambda = \Delta t/\Delta x$, $U_j^n = (1/\Delta x)\int_{x_{j-1/2}}^{x_{j+1/2}} U(x, t_n)\,\mathrm{d}x$.

If $\lambda_1 < \lambda_2 < \lambda_3 \leqslant 0$ or $0 \leqslant \lambda_1 < \lambda_2 < \lambda_3$ is satisfied, the Godunov numerical flux $F^G(U_j^n, U_{j+1}^n)$ is $F(U_{j+1}^n)$ or $F(U_j^n)$. When $\lambda_1 < 0$ and $\lambda_3 > 0$ are given, the Godunov numerical flux $F^G(U_j^n, U_{j+1}^n)$ is $F(V(0; U_j^n, U_{j+1}^n))$. In order to know $V(0; U_j^n, U_{j+1}^n)$, we must compute the exact or approximate solution to the RP.

Van Leer [13, 14] has extended Godunov's approach to the high-order MUSCL scheme. This high-order Godunov-type scheme in which the piecewise constants are replaced by piecewise linear data is now rewritten as follows:

$$U_j^{n+1} = U_j^n - \lambda(F_{j+1/2}^M - F_{j-1/2}^M)$$

$F_{j+1/2}^M$ is the same as that in the Godunov method, namely, $F_{j+1/2}^M = F(V(0; \bar{U}_{j+1/2}^{\mathrm{L}}, \bar{U}_{j+1/2}^{\mathrm{R}}))$. Here, $\bar{U}_{j+1/2}^{\mathrm{L}}$ and $\bar{U}_{j+1/2}^{\mathrm{R}}$ denote the initial values of the RP at $x_{j+1/2}$, which is

$$\bar{U}_{j+1/2}^{\mathrm{L}} = U_j^{\mathrm{R}} + \frac{1}{2}\frac{\Delta t}{\Delta x}[F(U_j^{\mathrm{L}}) - F(U_j^{\mathrm{R}})], \quad x < x_{j+1/2}$$

$$\bar{U}_{j+1/2}^{\mathrm{R}} = U_{j+1}^{\mathrm{L}} + \frac{1}{2}\frac{\Delta t}{\Delta x}[F(U_{j+1}^{\mathrm{L}}) - F(U_{j+1}^{\mathrm{R}})], \quad x > x_{j+1/2}$$

where $U_j^{\mathrm{L}} = U_j^n - \frac{1}{2}\Delta_j$ and $U_j^{\mathrm{R}} = U_j^n + \frac{1}{2}\Delta_j$. Δ_j is a suitably chosen slope vector of $U_j(x)$ in cell $[x_{j-1/2}, x_{j+1/2}]$. In this paper, we take the min-mod slope limiter which restrains oscillations and has more dissipation.

The piecewise parabolic method (PPM) method [15] is another high-order Godunov-type scheme which uses piecewise parabolic-limited reconstruction to obtain states to be used in the RPs defining the fluxes. WENO scheme [16] which will be used with the new solver is a fifth-order scheme. This is an improvement on the ENO scheme [17] of Harten and Osher.

2.3. The new solver

From a numerical point of view, it is very easy to compute a Godunov numerical flux when $\lambda_1 < \lambda_2 < \lambda_3 \leqslant 0$ or $0 \leqslant \lambda_1 < \lambda_2 < \lambda_3$, because of the simplicity of the solution to the RP in this case. Our main idea is to transform the systems which have general characteristic waves to that connected

Copyright © 2007 John Wiley & Sons, Ltd.

DOI: 10.1002/fld

to the case of $\lambda_1<\lambda_2<\lambda_3\leqslant 0$ or $0\leqslant\lambda_1<\lambda_2<\lambda_3$ in order to compute the numerical flux easily. A linear advection term is added to the flux functions in the first step to compute the numerical flux; then the effect of the added term is eliminated in the second step.

The original equation (1) is rewritten as follows:

$$\frac{\partial U}{\partial t}+\frac{\partial F_1(U)}{\partial x}+\frac{\partial F_2(U)}{\partial x}=0$$
$$U(x,0)=\begin{cases}U_{\mathrm{L}}, & x<0\\ U_{\mathrm{R}}, & x>0\end{cases} \tag{2}$$

where $F_1(U)=F(U)+WU$, $F_2(U)=-WU$ and W is a constant. In (2), we must make the eigenvalues of $F_1(U)$ and $F_2(U)$ all negative or positive. Based on the operator splitting method, given the value of $U(x,t)$ at t_n, in a time interval $(t_n, t_{n+1}]$, we split problem (2) into the next two problems:

$$\frac{\partial V}{\partial t}+\frac{\partial F_1(V)}{\partial x}=0$$
$$V(x,t_n)=U(x,t_n)=\begin{cases}U_{\mathrm{L}}, & x<0\\ U_{\mathrm{R}}, & x>0\end{cases} \tag{3}$$

$$\frac{\partial U}{\partial t}+\frac{\partial F_2(U)}{\partial x}=0$$
$$U(x,t_n)=V(x,t_{n+1}) \tag{4}$$

Then we compute the two problems in the time interval $(t_n, t_{n+1}]$ in turn and regard this solution as an approximate one to the solution of the original problem (1). The first step is to compute the Godunov numerical flux in problem (3) and the second step is to perform the same work in problem (4) using the numerical results in the first step.

The eigenvalues of the new flux $F_1(U)$ are $\tilde{\lambda}_1<\tilde{\lambda}_2<\tilde{\lambda}_3\leqslant 0$ or $0\leqslant\tilde{\lambda}_1<\tilde{\lambda}_2<\tilde{\lambda}_3$ (the structure of the solution to problem (3), see Figures 2 and 3). At the moment, the Godunov numerical flux of $F_1(U)$ is $F_1(U_{\mathrm{R}})$ or $F_1(U_{\mathrm{L}})$. Because problem (4) are linear advection systems with the case of $\hat{\lambda}_1=\hat{\lambda}_2=\hat{\lambda}_3=W$, we can easily derive that $F_2(V)$ is $F_2(V_{\mathrm{L}})$ or $F_2(V_{\mathrm{R}})$ correspondingly, where V is the value of U computed in the first step.

Because $\tilde{\lambda}_i=\lambda_i+W$ and $\tilde{\lambda}_i\leqslant 0$ or $0\leqslant\tilde{\lambda}_i$ $(i=1,2,3)$, the value of W depends on the λ_1 and λ_3. W is proposed to satisfy $\max(\lambda_1,\lambda_2,\lambda_3)+W\leqslant 0$ (as shown in Figure 2) or $0\leqslant\min(\lambda_1,\lambda_2,\lambda_3)+W$ (as shown in Figure 3). In order to reduce the effect on the time step as far as possible, we take

$$W=\begin{cases}0 & \text{if } \lambda_1\lambda_3>0\\ -\lambda_1 & \text{if } \lambda_1\lambda_3<0,\ \ |\lambda_1|<|\lambda_3|\\ -\lambda_3 & \text{if } \lambda_1\lambda_3<0,\ \ |\lambda_1|>|\lambda_3|\end{cases} \tag{5}$$

where $|\cdot|$ is the absolute value.

Suppose Δt_1, Δt_3 and Δt_4 are the time-step lengths determined by Courant–Friedrichs–Lewy (CFL) condition of problem (1), (3) and (4), respectively, then $\max(|\lambda_1|,|\lambda_2|,|\lambda_3|)\Delta t_1/\Delta x=\mathrm{cfl}<1$, $\max(|\tilde{\lambda}_1|,|\tilde{\lambda}_2|,|\tilde{\lambda}_3|)\Delta t_3/\Delta x=\mathrm{cfl}<1$, $\max(|\hat{\lambda}_1|,|\hat{\lambda}_2|,|\hat{\lambda}_3|)\Delta t_4/\Delta x=|W|\Delta t_4/\Delta x=\mathrm{cfl}<1$. Because

Copyright © 2007 John Wiley & Sons, Ltd.

DOI: 10.1002/fld

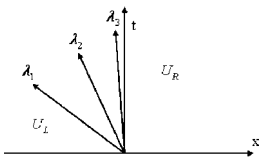

Figure 2. The structure of the solution of the Riemann problem (3).

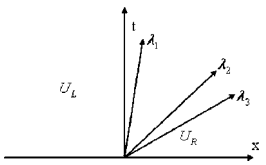

Figure 3. The structure of the solution of the Riemann problem (3).

$|W| < \max(|\lambda_1|, |\lambda_2|, |\lambda_3|)$, we can show that the time step of problem (3) can be no less than half of that of the original method (1) as follows:

$$\begin{aligned}\max(|\lambda_1 + W|, |\lambda_2 + W|, |\lambda_3 + W|) &\leqslant \max(|\lambda_1| + |W|, |\lambda_2| + |W|, |\lambda_3| + |W|)\\ &= |W| + \max(|\lambda_1|, |\lambda_2|, |\lambda_3|)\\ &\leqslant 2\max(|\lambda_1|, |\lambda_2|, |\lambda_3|)\end{aligned}$$

that means

$$\frac{\max(|\lambda_1|, |\lambda_2|, |\lambda_3|)}{\max(|\tilde{\lambda}_1|, |\tilde{\lambda}_2|, |\tilde{\lambda}_3|)} \geqslant \frac{1}{2}$$

$$\max(\Delta t_3, \Delta t_4) \geqslant \tfrac{1}{2}\Delta t_1$$

We obtain that the time interval $[t_n, t_{n+1}]$ in the two-step splitting method is not less than $\frac{1}{2}$ that of Δt_1 in the original method under condition (5).

Since we do not want to compute the exact solution of the RP (1) to obtain the value of W exactly, we have to find some kinds of approximation to λ_1 and λ_3. Denote λ_L and λ_R as the approximation of λ_1 and λ_3, respectively. Before performing some estimates of λ_L and λ_R, we only know the values of U_L and U_R in the original RP (1). Hence, we can compute the values of u which is the velocity and a which is the local sound speed on both sides of the discontinuity, where u_R, a_R, u_L, a_L denote the corresponding values. In this paper, six estimates of the approximate λ_1 and λ_3 are given. The simple estimates are

$$\lambda_L = u_L - a_L, \quad \lambda_R = u_R + a_R \tag{6}$$

$$\lambda_L = \tfrac{1}{2}(u_L + u_R) - \tfrac{1}{2}(a_L + a_R), \quad \lambda_R = \tfrac{1}{2}(u_L + u_R) + \tfrac{1}{2}(a_L + a_R) \tag{7}$$

and

$$\lambda_L = \min(u_L - a_L, u_R - a_R), \quad \lambda_R = \max(u_L + a_L, u_R + a_R) \tag{8}$$

Copyright © 2007 John Wiley & Sons, Ltd.

DOI: 10.1002/fld

In most cases, the choices in (6) and (7) are good estimates. However, they may fail in some cases which will be seen in the blast wave test. The choice in (8) is robust and can be used broadly. Its main drawback is that it leads to a very large value of W that causes too much dissipation in the computation.

We also propose to use the Roe-average eigenvalues for the estimates, that is

$$\lambda_L = \tilde{u} - \tilde{a}, \quad \lambda_R = \tilde{u} + \tilde{a} \tag{9}$$

where $\tilde{u}$ and $\tilde{a}$ are the Roe-average velocity and the sound speed, respectively, which for an ideal-gas EOS are given as follows:

$$\tilde{u} = \frac{\sqrt{\rho_L}u_L + \sqrt{\rho_R}u_R}{\sqrt{\rho_L} + \sqrt{\rho_R}}, \quad \tilde{a} = \sqrt{(\gamma - 1)(\tilde{H} - \tfrac{1}{2}\tilde{u}^2)} \tag{10}$$

with the enthalpy $H = (E + p)/\rho$, approximated as

$$\tilde{H} = \frac{\sqrt{\rho_L}H_L + \sqrt{\rho_R}H_R}{\sqrt{\rho_L} + \sqrt{\rho_R}} \tag{11}$$

The choice of (9) is a very good one which leads to a robust method and can make the Riemann solver more accurate. In fact, we can get a variation of (9), that is

$$\lambda_L = \min(\tilde{u} - \tilde{a}, u_L - a_L), \quad \lambda_R = \max(\tilde{u} + \tilde{a}, u_R + a_R) \tag{12}$$

The last choice is given as follows:

$$\lambda_L = \tilde{u} - \tilde{d}, \quad \lambda_R = \tilde{u} + \tilde{d} \tag{13}$$

where $\tilde{u}$ is the Roe-average velocity

$$\tilde{d} = \frac{\sqrt{\rho_L}a_L^2 + \sqrt{\rho_R}a_R^2}{\sqrt{\rho_L} + \sqrt{\rho_R}} + \eta(u_R - u_L)^2 \tag{14}$$

and

$$\eta = \frac{1}{2}\frac{\sqrt{\rho_L}\sqrt{\rho_R}}{(\sqrt{\rho_L} + \sqrt{\rho_R})^2} \tag{15}$$

Which of the above estimates is the best for the new solver? We cannot answer this question in theory, since a lot of numerical tests show that (13) is robust and its dissipation is small. Some remarks and analysis about the above six choices are shown in Section 3.

As for problem (4), the equations are linear advection systems and can be easily computed numerically by the same scheme. In this way, we find an approximate solution to the RP of the Euler equations in fluid mechanics.

In order to implement the new two-step splitting Riemann solver in the Godunov method, one performs the following steps:

(a) Compute the wave speeds λ_L and λ_R according to any of the (6)–(9), (12) and (13).
(b) If $0 \leqslant \lambda_L < \lambda_R$, go to Step (c). If $\lambda_L < \lambda_R \leqslant 0$, go to Step (d). If $\lambda_L < 0 < \lambda_R$, go to Step (e).
(c) Compute the cell average at the next time level using the Godunov numerical flux,

$$U_j^{n+1} = U_j^n - \lambda(F(U_j^n) - F(U_{j-1}^n)) \tag{16}$$

Copyright © 2007 John Wiley & Sons, Ltd.

DOI: 10.1002/fld

(d) Compute the cell average at the next time level using the Godunov numerical flux,

$$U_j^{n+1} = U_j^n - \lambda(F(U_{j+1}^n) - F(U_j^n)) \tag{17}$$

(e) Compute W using (5). If $W>0$,

$$\begin{aligned} V_j^{n+1} &= U_j^n - \lambda(F_1(U_j^n) - F_1(U_{j-1}^n)) \\ U_j^{n+1} &= V_j^{n+1} - \lambda(F_2(V_{j+1}^{n+1}) - F_2(V_j^{n+1})) \end{aligned} \tag{18}$$

If $W<0$,

$$\begin{aligned} V_j^{n+1} &= U_j^n - \lambda(F_1(U_{j+1}^n) - F_1(U_j^n)) \\ U_j^{n+1} &= V_j^{n+1} - \lambda(F_2(V_j^{n+1}) - F_2(V_{j-1}^{n+1})) \end{aligned} \tag{19}$$

3. NEW RIEMANN SOLVER IN EULER EQUATIONS FOR IDEAL GASES

Here, we present some numerical tests to show that the Riemann solver is robust and some descriptions of comparisons between various given λ_L, λ_R values. The new solver with second-order MUSCL and WENO fifth-order data reconstruction achieves high-resolution Godunov-type method. We take several well-known problems from the related literature, which have the following Riemann-type initial conditions:

$$U(x,0) = \begin{cases} U_L, & x<x_0 \\ U_R, & x>x_0 \end{cases}$$

We compare Godunov scheme and MUSCL scheme with the new Riemann solver and with the exact Riemann solver. The new Riemann solver does not need an iterative technique and the codes can be written easily. Compared with the exact Riemann solver, the Godunov scheme with the new Riemann solver which has only first-order accuracy has a little higher dissipation. However, the MUSCL scheme shows good accuracy compared with that of an exact Riemann solver. We also see that the new solver with WENO data reconstruction and 3-order Runge–Kutta method in time can achieve more accuracy. In the following tests, the two-step splitting solver is shown to deal with the whole range of cases from sonic rarefaction waves, strong shocks, slow shocks and so on.

CFL numbers are 0.9, 0.8, 0.4 in the Godunov scheme, MUSCL schemes and WENO scheme, respectively.

3.1. Modified Sod's shock tube [*18*]

The initial conditions in this test are given by

$$(\rho, u, p)_L = (1.0, 0.75, 1.0)$$
$$(\rho, u, p)_R = (0.125, 0.0, 0.1)$$

Copyright © 2007 John Wiley & Sons, Ltd.

DOI: 10.1002/fld

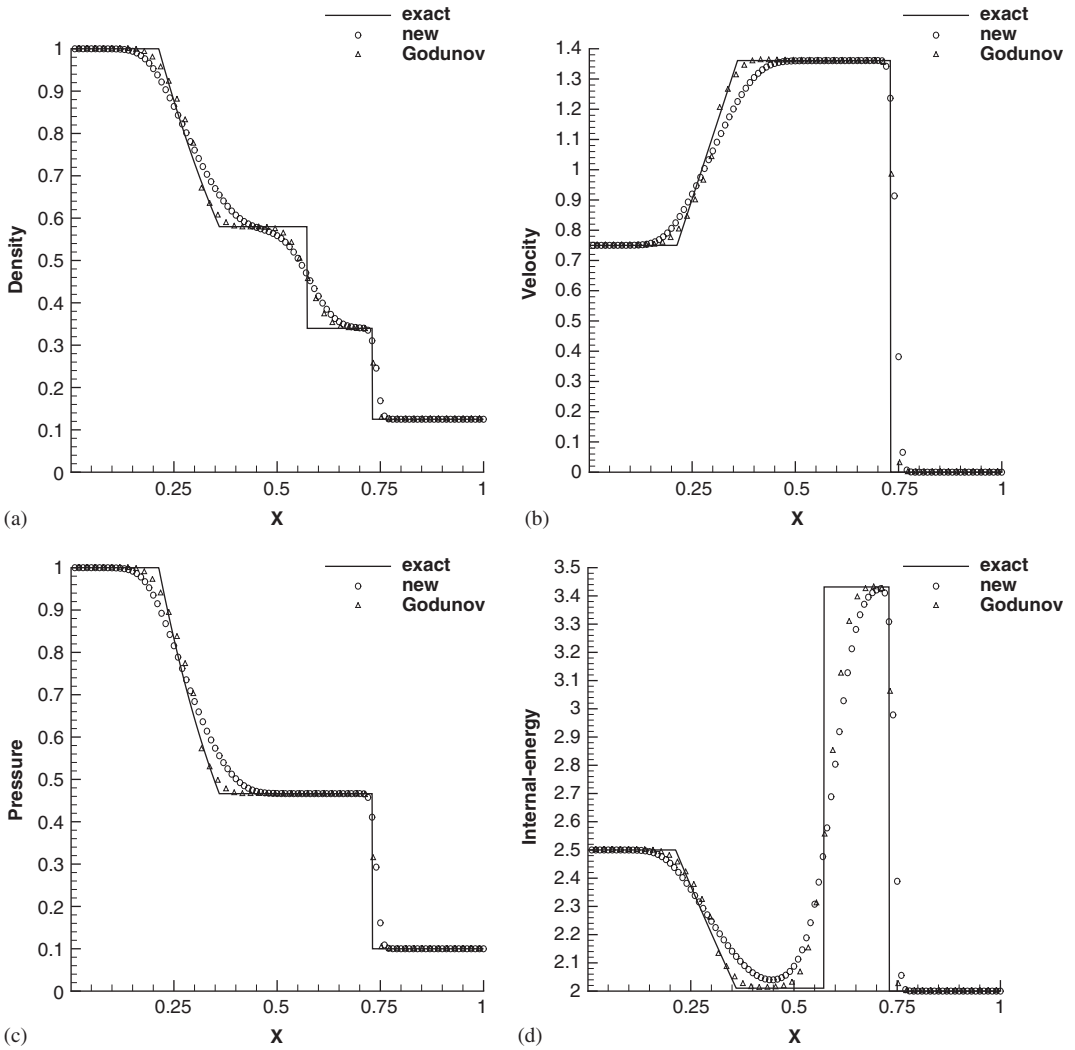

Figure 4. Test 3.1 Godunov scheme (100 grids, $t = 0.2$) with the new solver (new) and the exact solver (Godunov) and the initial discontinuous point is 0.3: (a) density; (b) velocity; (c) pressure; and (d) internal-energy.

The solution to this test consists of a right shock wave, a right traveling contact wave and a left sonic rarefaction wave; this test is very useful in assessing the entropy satisfaction property of numerical methods. Because in the two-step splitting method there are no sonic points in both the first system of equations and the second system of equations, the sonic point glitch phenomena will not happen in this test. The current solver is better than the exact solver and the Roe solver; both have the sonic glitch in the test as shown in Figure 4. The grids used in the MUSCL scheme and the Godunov scheme contain 100 cells. The density numerical results of the MUSCL scheme with the new Riemann solver are as good as that with the exact Riemann solver shown in Figure 5.

Copyright © 2007 John Wiley & Sons, Ltd.

DOI: 10.1002/fld

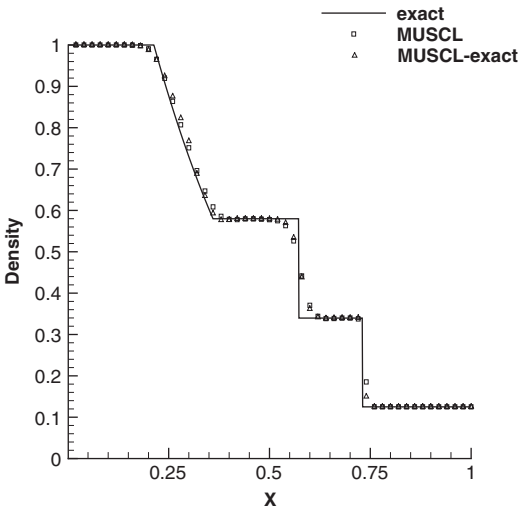

Figure 5. Test 3.1 MUSCL scheme with the new solver (new) and the exact solver (MUSCL) (100 grids): (a) density.

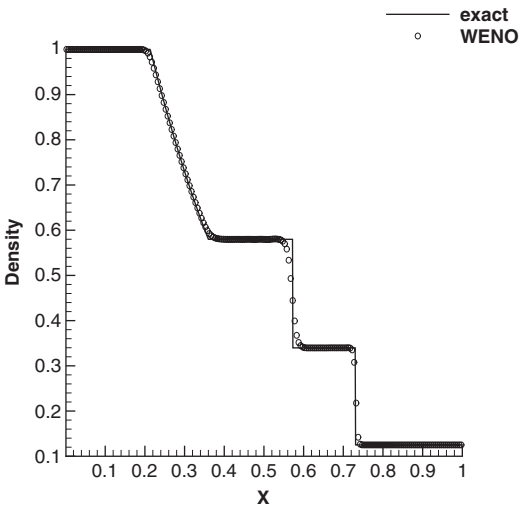

Figure 6. Test 3.1 WENO scheme with the new solver (200 grids): (a) density.

In Figure 6 (200 cells), we show the numerical result computed by the WENO scheme with the new solver.

3.2. Blast wave [*19*]

This test is a very severe problem and is designed to test the robustness of the Godunov-type method. Its solution consists of a right strong shock wave, a contact surface and a left rarefaction

Copyright © 2007 John Wiley & Sons, Ltd.

DOI: 10.1002/fld

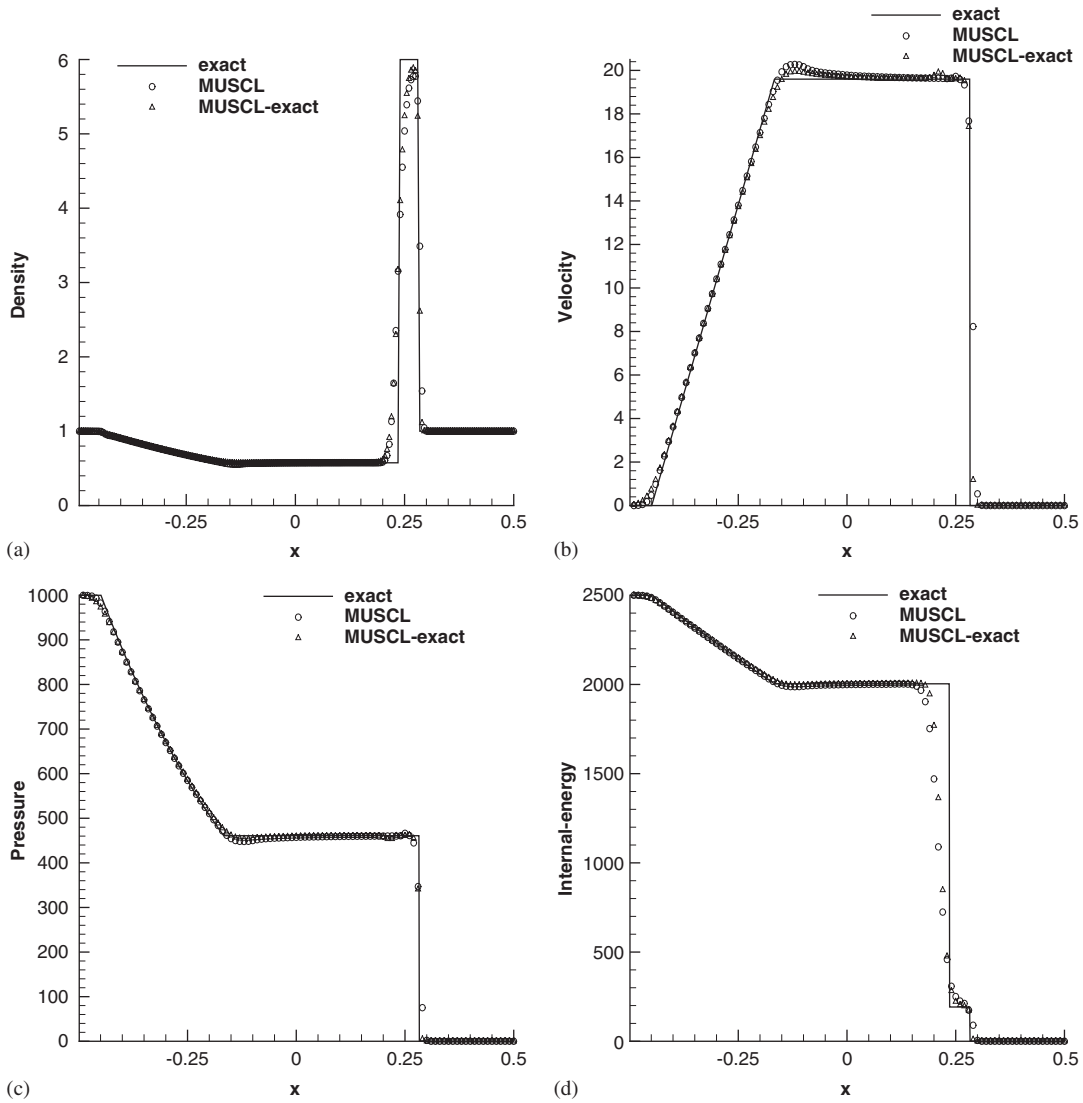

Figure 7. Test 3.2 MUSCL scheme (200 grids, $t = 0.012$) with the new solver (MUSCL) and the exact solver (MUSCL-exact) and the initial discontinuous point is 0.0: (a) density; (b) velocity; (c) pressure; and (d) internal-energy.

wave. The numerical results of this problem are shown in Figure 7, where the right traveling shock wave has a pressure ratio of 46 000 and a corresponding shock Mach number of 198. Its initial conditions may be given as follows:

$$(\rho, u, p)_{\mathrm{L}} = (1.0, 0.0, 1000)$$

$$(\rho, u, p)_{\mathrm{R}} = (1.0, 0.0, 0.01)$$

Copyright © 2007 John Wiley & Sons, Ltd.

DOI: 10.1002/fld

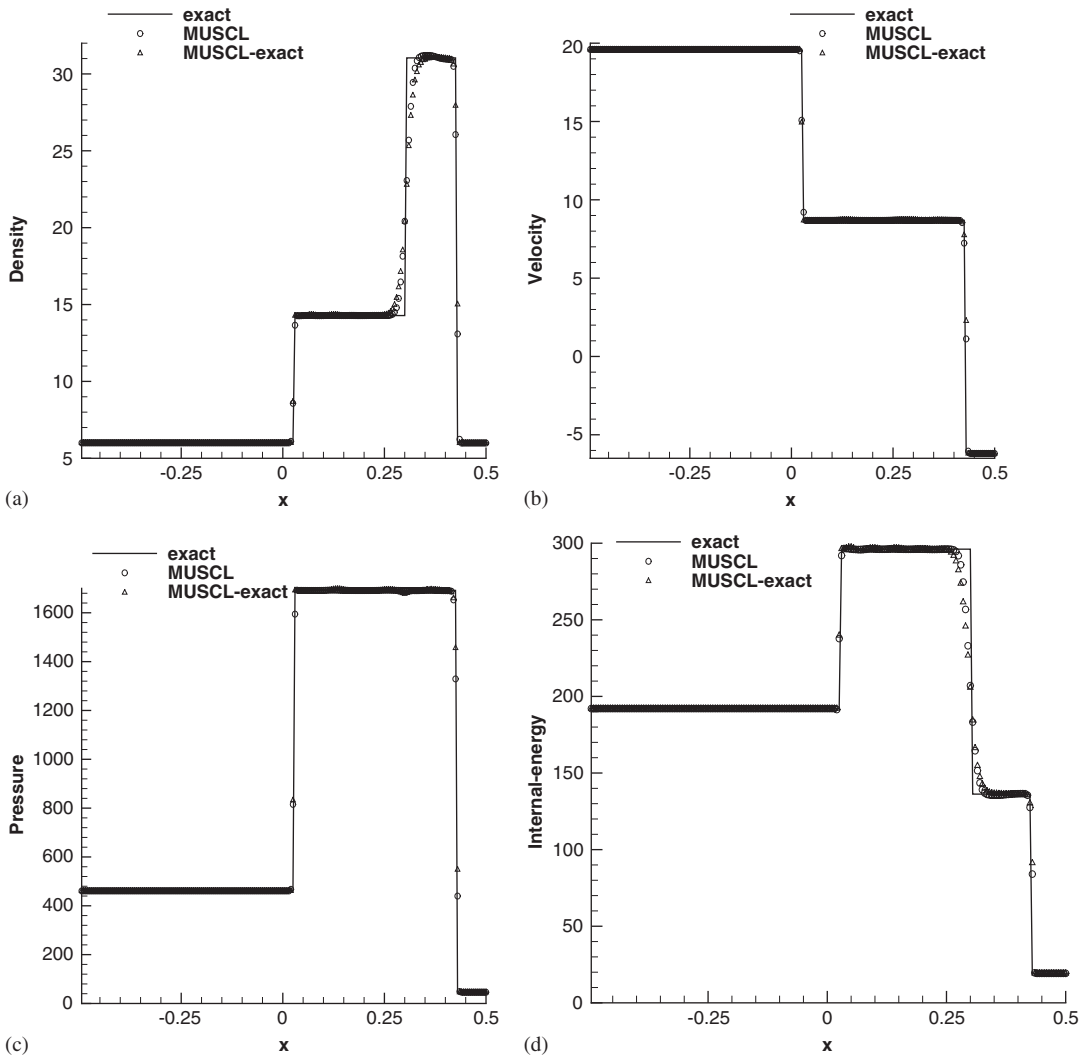

Figure 8. Test 3.3 MUSCL scheme (200 grids, $t = 0.035$) with the new solver (MUSCL) and the exact solver (MUSCL-exact) and the initial discontinuous point is 0.0: (a) density; (b) velocity; (c) pressure; and (d) internal-energy.

The MUSCL scheme shows its robustness and accuracy in the test. The number of grids used in the new Riemann solver and the exact Riemann solver are both 200.

3.3. Slowly moving shock wave [*20*]

The solution of this test consists of three discontinuities: two shock waves and a contact wave. The three waves all travel to the right and the left shock's speed is very slow. However, the right

Copyright © 2007 John Wiley & Sons, Ltd.

DOI: 10.1002/fld

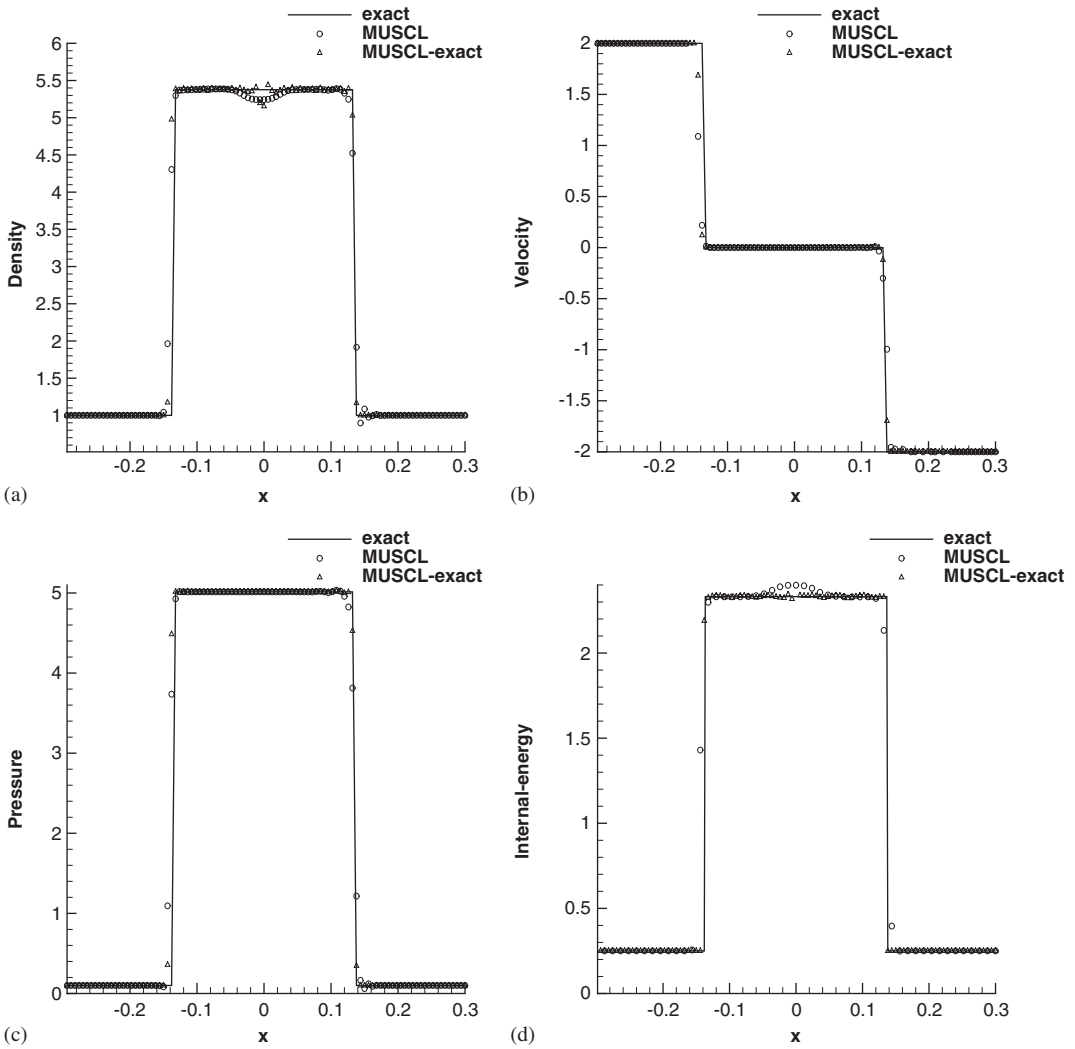

Figure 9. Test 3.4 MUSCL scheme (100 grids, $t = 0.3$) with the new solver (MUSCL) and the exact solver (MUSCL-exact) and the initial discontinuous point is 0.0: (a) density; (b) velocity; (c) pressure; and (d) internal-energy.

shock wave propagates very fast. The initial conditions may be given as follows:

$$(\rho, u, p)_{\mathrm{L}} = (5.99924, 19.5975, 460.894)$$

$$(\rho, u, p)_{\mathrm{R}} = (5.99242, -6.19633, 46.095)$$

From Figure 8, there are some low spurious oscillations in the left shock wave in internal energy in the MUSCL scheme with the exact Riemann solver, but almost no oscillation is seen from the

Copyright © 2007 John Wiley & Sons, Ltd.

DOI: 10.1002/fld

Table I. Test 3.1 density, velocity and pressure L_1 errors for the Godunov scheme with the exact Riemann solver and the new solver in different scales of grids.

Test 3.1	100	200	400	800	1600
Exact density	1.373225E−2	9.150315E−3	6.119587E−3	4.097982E−3	2.657459E−3
New density	1.740888E−2	1.133677E−2	7.744048E−3	5.022129E−3	3.282395E−3
Exact velocity	2.081570E−2	1.165704E−2	6.701308E−3	4.007716E−3	1.779287E−3
New velocity	2.286901E−2	1.125322E−2	7.807958E−3	4.054747E−3	1.996814E−3
Exact pressure	8.865263E−3	5.297864E−3	3.188550E−3	1.946960E−3	1.027800E−3
New pressure	1.137116E−2	6.538917E−3	4.184224E−3	2.354250E−3	1.321964E−3

Table II. Test 3.2 density, velocity and pressure L_1 errors for the MUSCL scheme with the exact Riemann solver and the new solver in different scales of grids.

Test 3.2	100	200	400	800	1600
Exact density	0.151889	9.146613E−2	5.360357E−2	3.286152E−2	1.923284E−2
New density	0.181654	0.104402	5.730914E−2	3.203123E−2	1.645971E−2
Exact velocity	0.471223	0.264751	0.166156	7.325079E−2	5.674742E−2
New velocity	0.580808	0.320305	0.179986	8.868734E−2	4.121640E−2
Exact pressure	9.453613	5.291827	3.414134	1.481660	1.123664
New pressure	10.527827	6.014166	3.529512	1.728326	0.808145

Table III. Test 3.3 density, velocity and pressure L_1 errors for the MUSCL scheme with the exact Riemann solver and the new solver in different scales of grids.

Test 3.3	100	200	400	800	1600
Exact density	0.765504	0.421964	0.200816	0.112398	6.768651E−2
New density	0.708083	0.369238	0.187838	8.727035E−2	5.037989E−2
Exact velocity	0.348780	0.149468	4.959207E−2	2.163093E−2	1.073556E−2
New velocity	0.328804	0.141722	6.241415E−2	2.149678E−2	1.138103E−2
Exact pressure	33.927291	15.095404	4.944796	2.385813	1.328164
New pressure	32.572240	13.734135	5.766796	2.138337	1.182284

Table IV. Test 3.4 density, velocity and pressure L_1 errors for the MUSCL scheme with the exact Riemann solver and the new solver in different scales of grids.

Test 3.4	100	200	400	800	1600
Exact density	3.464184E−2	1.765690E−2	1.036847E−2	6.440046E−3	4.483109E−3
New density	5.030778E−2	2.468025E−2	1.136775E−2	6.165262E−3	3.021769E−3
Exact velocity	1.582973E−2	6.065832E−3	3.049358E−3	1.655456E−3	7.600848E−4
New velocity	2.424175E−2	1.077308E−2	4.257351E−3	2.963712E−3	1.287112E−3
Exact pressure	3.327922E−2	1.536902E−2	8.152541E−3	3.946913E−3	1.968046E−3
New pressure	4.598175E−2	2.197651E−2	1.008105E−2	5.716547E−3	1.757348E−3

result of the MUSCL scheme with the new Riemann solver. We think the dissipation in the new solver diminishes the oscillations. The grid in figures contains 200 cells.

Copyright © 2007 John Wiley & Sons, Ltd.

DOI: 10.1002/fld

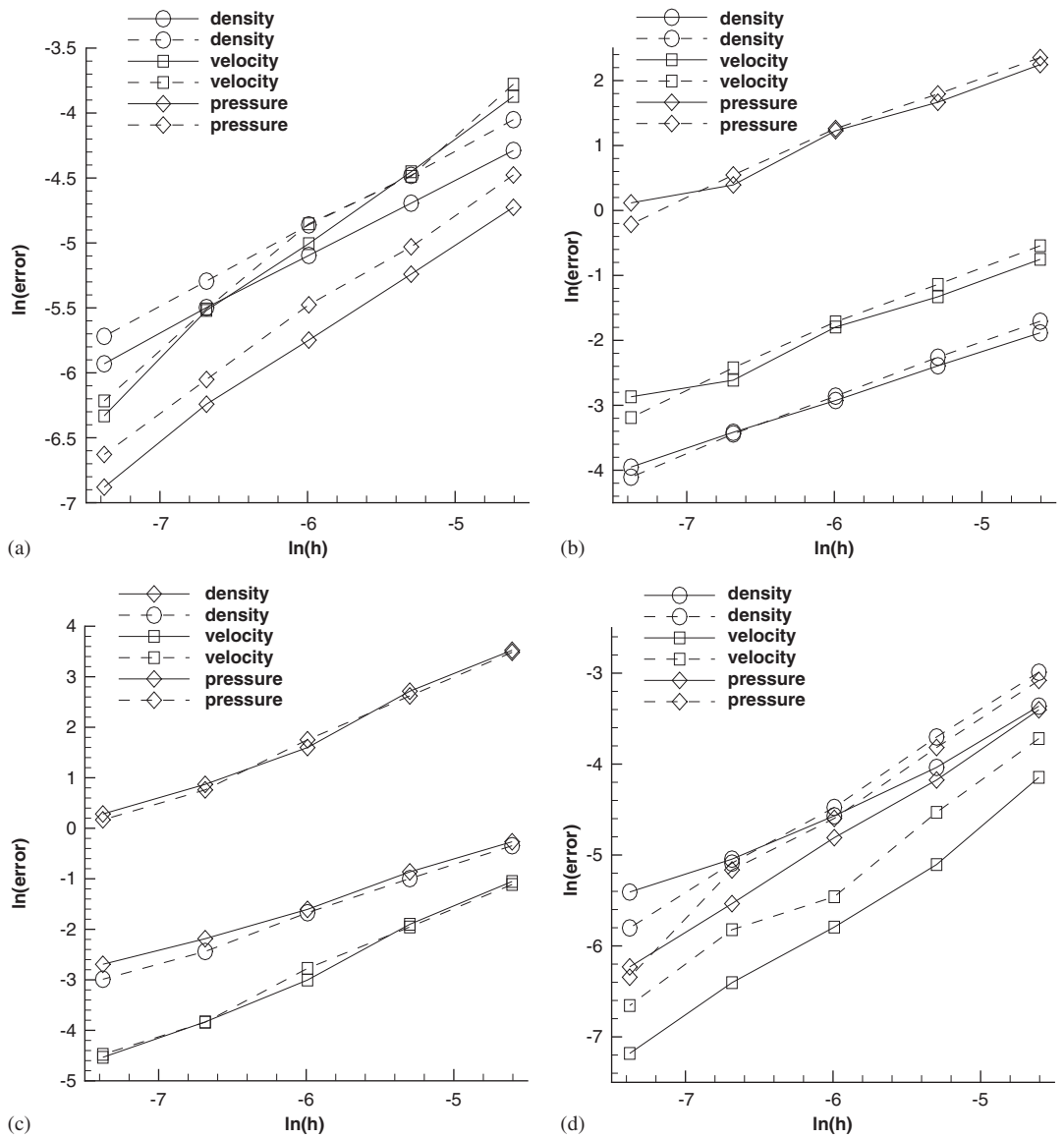

Figure 10. L1 convergence in MUSCL scheme with the exact Riemann solver (solid lines) and the new solver (dashed lines): (a) test 3.1; (b) test 3.2; (c) test 3.3; and (d) test 3.4.

3.4. Osher colliding shock waves [*3*]

The initial conditions may be given as follows:

$$(\rho, u, p)_{\mathrm{L}} = (1.0, 2.0, 0.1)$$

$$(\rho, u, p)_{\mathrm{R}} = (1.0, -2.0, 0.1)$$

Copyright © 2007 John Wiley & Sons, Ltd.

DOI: 10.1002/fld

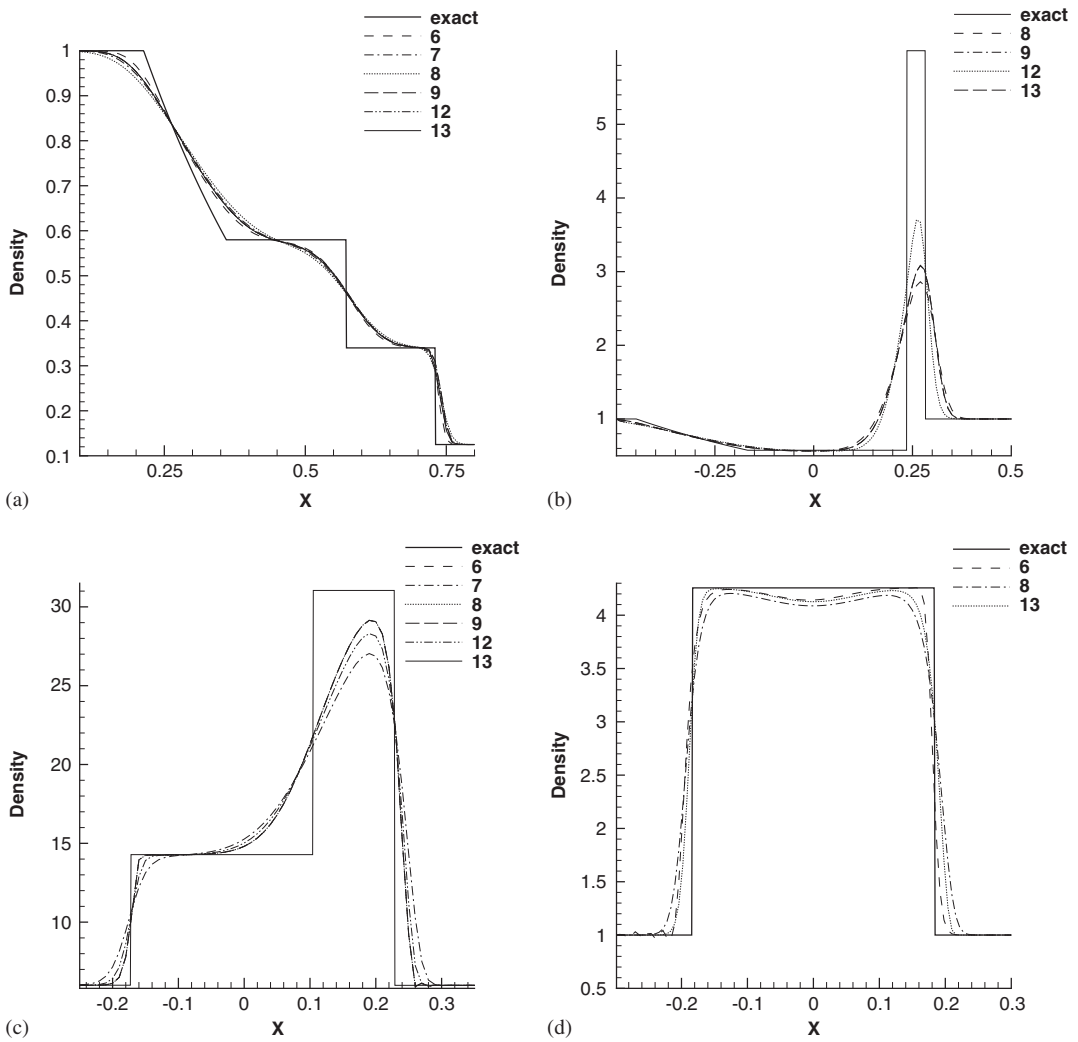

Figure 11. Comparison of six estimates of the approximate λ_1 and λ_3: (a) test 3.1; (b) test 3.2; (c) test 3.3; and (d) test 3.4.

This test simulates the collision of two flows. Its solution consists of two symmetric strong shock waves and a stationary contact wave. This is similar to the slowly moving shock waves test where some spurious oscillations are seen in the contact wave in density and internal energy. This phenomenon is the so-called wall-heating problem. The results are shown in Figure 9. Because of dissipation, the new solver works better than the exact solver. The end time is 0.3 and the grid contains 100 cells in the MUSCL scheme.

For the above four tests we can compare the errors of the numerical solutions using the exact solutions. Tables I–IV summarize L_1 errors of the numerical solutions in density, velocity and pressure of these tests. The grids used contain 100, 200, 400, 800, 1600 cells for all tests which

Copyright © 2007 John Wiley & Sons, Ltd.

DOI: 10.1002/fld

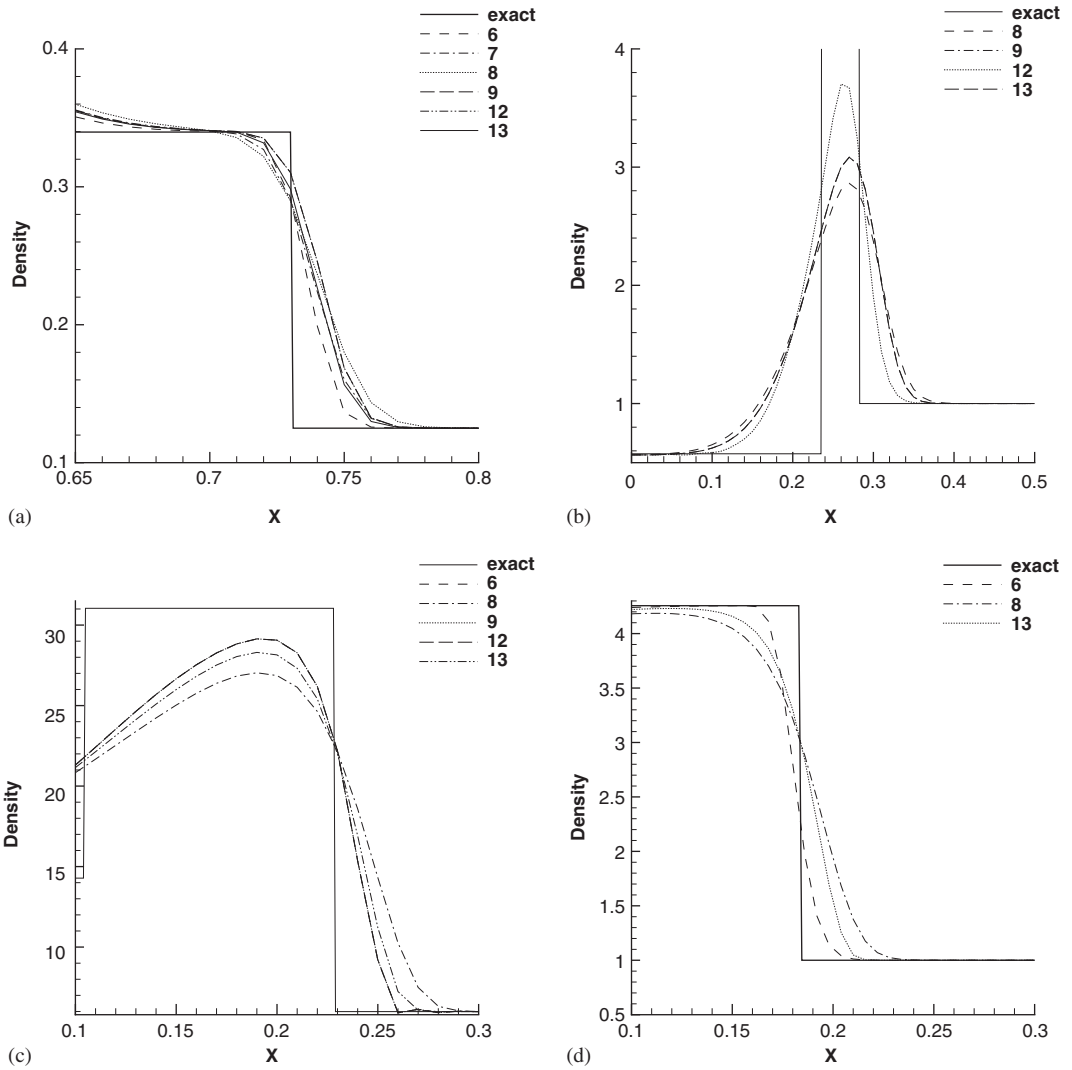

Figure 12. Comparison of six estimates of the approximate λ_1 and λ_3: (a) test 3.1; (b) test 3.2; (c) test 3.3; and (d) test 3.4.

were computed by the MUSCL scheme with the exact Riemann solver and the new solver, except Table I where the results were computed by Godunov scheme. In Tables I–IV, 'new' denotes the results of new solver and 'exact' denotes the results of the exact Riemann solver. All these results can be seen in Figure 10, where h is Δx.

In Section 2.3, we give six estimates to approximate λ_1 and λ_3. Here, we review the behavior of these estimates in the above four numerical tests. All the numerical results of different estimates can be seen in Figures 11 and 12, and both of the figures contain four sub-figures which denote

Copyright © 2007 John Wiley & Sons, Ltd.

DOI: 10.1002/fld

test 1, test 2, test 3 and test 4, respectively. Figure 11 shows the numerical results for the density; local structures of the tests can be seen in Figure 12. All choices can be applied successfully in test 1. Choice (6) failed in test 2, choice (7) failed in test 2, test 3 and test 4, choice (8) and choice (13) can be applied to all tests successfully, choice (9) and choice (12) only failed in test 4. In test 1 choice (9) and choice (12) are the same, in test 2 choice (9) and choice (13) are the same, in test 3 choice (6), choice (8) and choice (12) are the same. Choice (12) and choice (13) have small dissipation and choice (8) is on the contrary. From Figures 11 and 12, we conclude that choice (8), choice (9) and choice (13) are all recommended. Considering accuracy and robustness, choice (13) is the better choice.

4. NEW RIEMANN SOLVER IN EULER EQUATIONS OF COMPLEX EQUATION OF STATE

In this section, three EOS for the Euler equations will be considered: Tammann EOS, Binomial gas EOS and van der Waals EOS. The Tammann EOS [21] is suitable for describing liquid at high pressure and flows undergoing non-isentropic process, such as shock waves. A review of similar EOS for a liquid can be found in Reference [22].

The EOS formula can be represented as follows:

$$p = p(\rho, e) = (\gamma - 1)\rho e - \gamma p_c \tag{20}$$

where p, ρ and e are the pressure, density and internal energy, respectively. The values for the pressure constant p_c and polytropic constant γ are liquid dependent and many of these values corresponding to a number of different liquids can be found in the literature. Note that if $1<\gamma<2$ and $p_c = 0$, the Tammann equation of state reduces to the ideal gas equation of state. We choose two conditions: one is $\gamma = 3$ and $p_c = 1$; another is $\gamma = 7.15$ and $p_c = 3309$, which describes water.

We also take the Binomial gas EOS, which can be written as follows:

$$p = [(\gamma - 1)e + c_0^2]\rho - \rho_0 c_0^2 \tag{21}$$

where p, ρ and e are the pressure, density and internal energy, respectively. The values of ρ_0 and c_0 are constants, γ is the polytropic constant.

van der Waals EOS is recalled below:

$$p = \left(\frac{\gamma - 1}{1 - b\rho}\right)(\rho e + a\rho^2) - a\rho^2 \tag{22}$$

so as to deal with the possible real-gas effect when both the temperature and pressure are high. Here, e denotes the internal energy, γ is the ratio of specific heat and the quantities a, b are van der Waals gas constants for molecular cohesive forces and the finite size of molecules, respectively ($a \geqslant 0$, $0 \leqslant b < 1/\rho$ [23]). Note that a van der Waals gas of the form (22) reduces to a Noble–Abel gas (a constant covolume gas) when $a = 0$ and to a polytropic gas when $b = 0$ as well. Here, we do not consider the phase transition of van der Waals EOS. The RP near phase transitions is an anomalous wave structure: either shock waves split into multiple waves, or composite waves form which will be seen in [12]. Our ongoing work concerns how to deal with these difficult problems.

Copyright © 2007 John Wiley & Sons, Ltd.

DOI: 10.1002/fld

Here, all CFL numbers are equal to 0.9.

4.1. Test 4.1

Test 1 is $\gamma = 3$ and $p_c = 1$. The initial values are given by the following:

$$(\rho, u, p)_L = (1.0, 0.0, 1.0)$$

$$(\rho, u, p)_R = (0.75, 0.0, 0.05)$$

The exact solution is composed of a left rarefaction wave, a right traveling strong contact and a right shock wave at the time $t = 0.15$. Because the rarefaction fan is narrow, it is a very severe problem for numerical methods. We show the results of the Godunov scheme, MUSCL scheme with the two-step splitting Riemann solver in Figure 13, where the grids used in the two schemes contain 100 cells.

4.2. Test 4.2: water

The values of γ and p_c in Tammann equation of state are 7.15 and 3309, respectively. Initial conditions are given as follows:

$$(\rho, u, p)_L = (1.0, 20, 1.0)$$

$$(\rho, u, p)_R = (1.0, 20, 1000)$$

The end time is equal to 0.01. The exact solution contains a right shock wave, a right slowly traveling contact wave and a left rarefaction wave. The rarefaction wave is so narrow that it is hard for the Godunov scheme to simulate the wave and the high-order schemes can give much better results. In fact, it is very difficult for water to be compressed even in the case of high pressure, so the density of water changes very slightly. We show the numerical results that are computed by the MUSCL scheme with the new Riemann solver in Figure 14. The grid used contains 200 cells.

4.3. Test 4.3: binomial gases

The constants ρ_0, γ and c_0 in the binomial gas are equal to 0.5, 1.4, 0.5 individually. The initial conditions are given by the following:

$$(\rho, u, p)_L = (1.0, 0.5, 1.0)$$

$$(\rho, u, p)_R = (0.125, 0.0, 0.1)$$

The solution of test 3 is similar to the modified Sod's shock tube, which consists of a left rarefaction wave, a contact wave and a right shock wave. We show the Godunov scheme and MUSCL scheme with the new Riemann solver in Figure 15 at the time $t = 0.2$, using 100 cells.

4.4. Test 4.4: van der Waals EOS

The values of the constants are as follows:

$$a = 1684.54, \quad b = 0.001692, \quad \gamma = 1.3292 \tag{23}$$

Copyright © 2007 John Wiley & Sons, Ltd.

DOI: 10.1002/fld

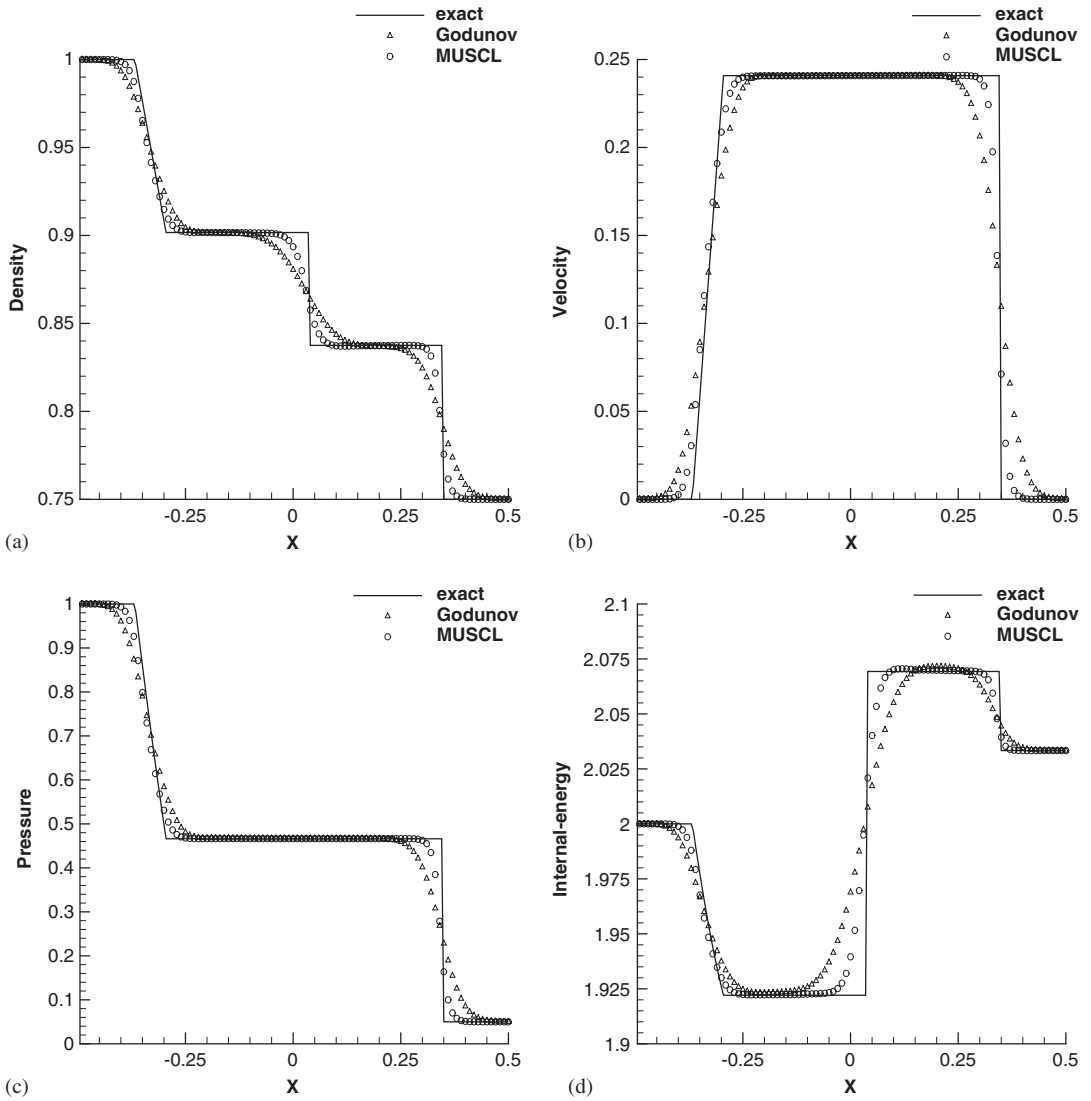

Figure 13. Test 4.1 Godunov scheme and MUSCL scheme with the new solver (100 grids, $t = 0.15$) and the initial discontinuous point is 0.0: (a) density; (b) velocity; (c) pressure; and (d) internal-energy.

and this test is from [8]. Initial conditions are given by the following:

$$(\rho, u, p)_{\mathrm{L}} = (250.0, 0.0, 35966778)$$

$$(\rho, u, p)_{\mathrm{R}} = (166.6, 0.0, 27114795)$$

The fluid stands everywhere in the gas phase. Profiles of density, velocity and pressure computed by the Godunov scheme and MUSCL scheme with the new solver are plotted in Figure 16 for the

Copyright © 2007 John Wiley & Sons, Ltd.

DOI: 10.1002/fld

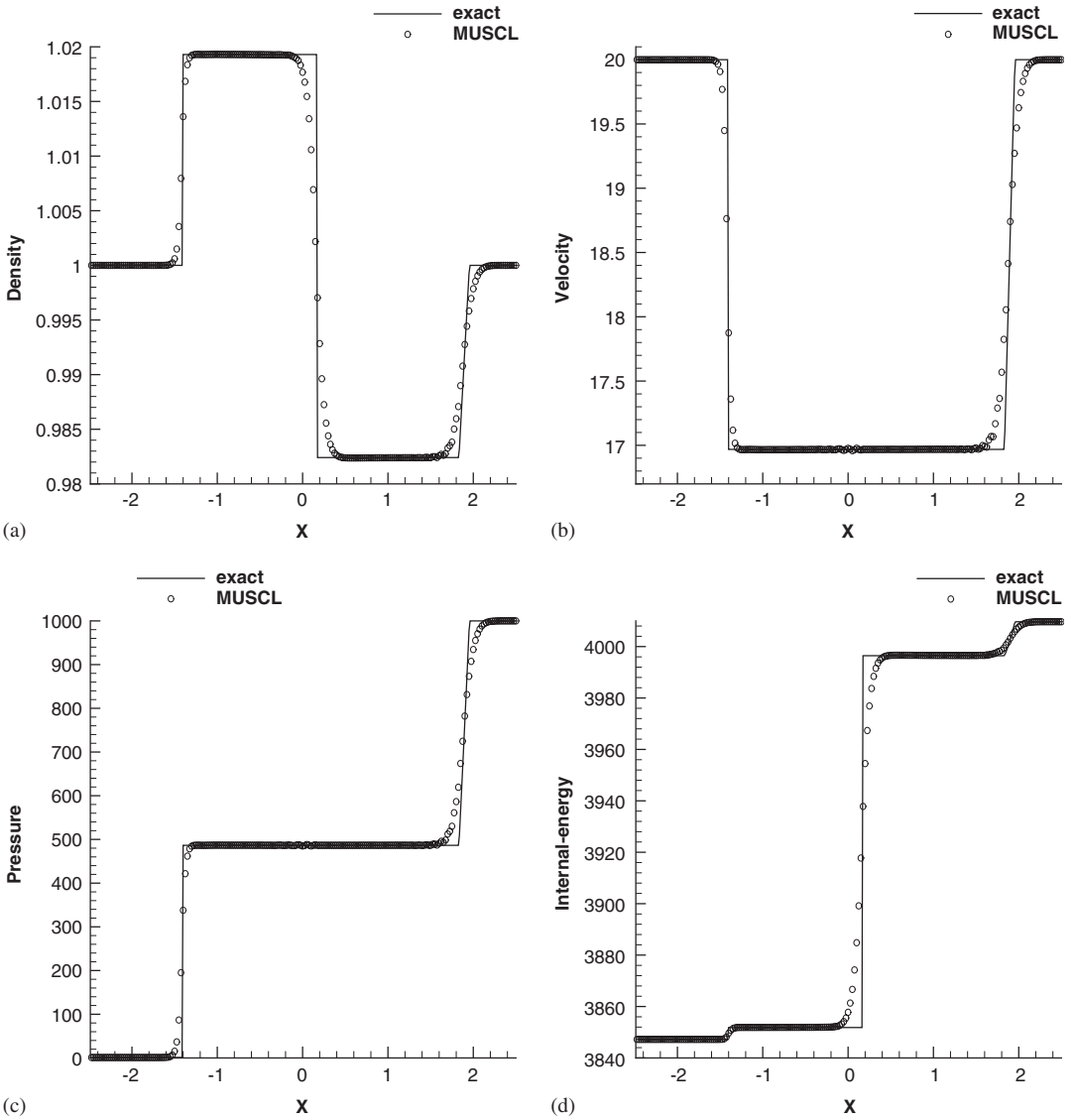

Figure 14. Test 4.2 MUSCL scheme with the new solver (200 grids, $t = 0.01$) and the initial discontinuous point is 0.0: (a) density; (b) velocity; (c) pressure; and (d) internal-energy.

case of using 200 cells, where the end time is 0.01. The numerical result of this test in accordance with the one of [8]. The new solver in Nobel–Abel gas simulation which is similar to van der Waals gas also proved successful in our numerical tests.

All of the above tests for the Euler equations of complex EOS prove that the new Riemann solver runs effectively in the Godunov scheme and MUSCL scheme. From the four tests, the numerical

Copyright © 2007 John Wiley & Sons, Ltd.

DOI: 10.1002/fld

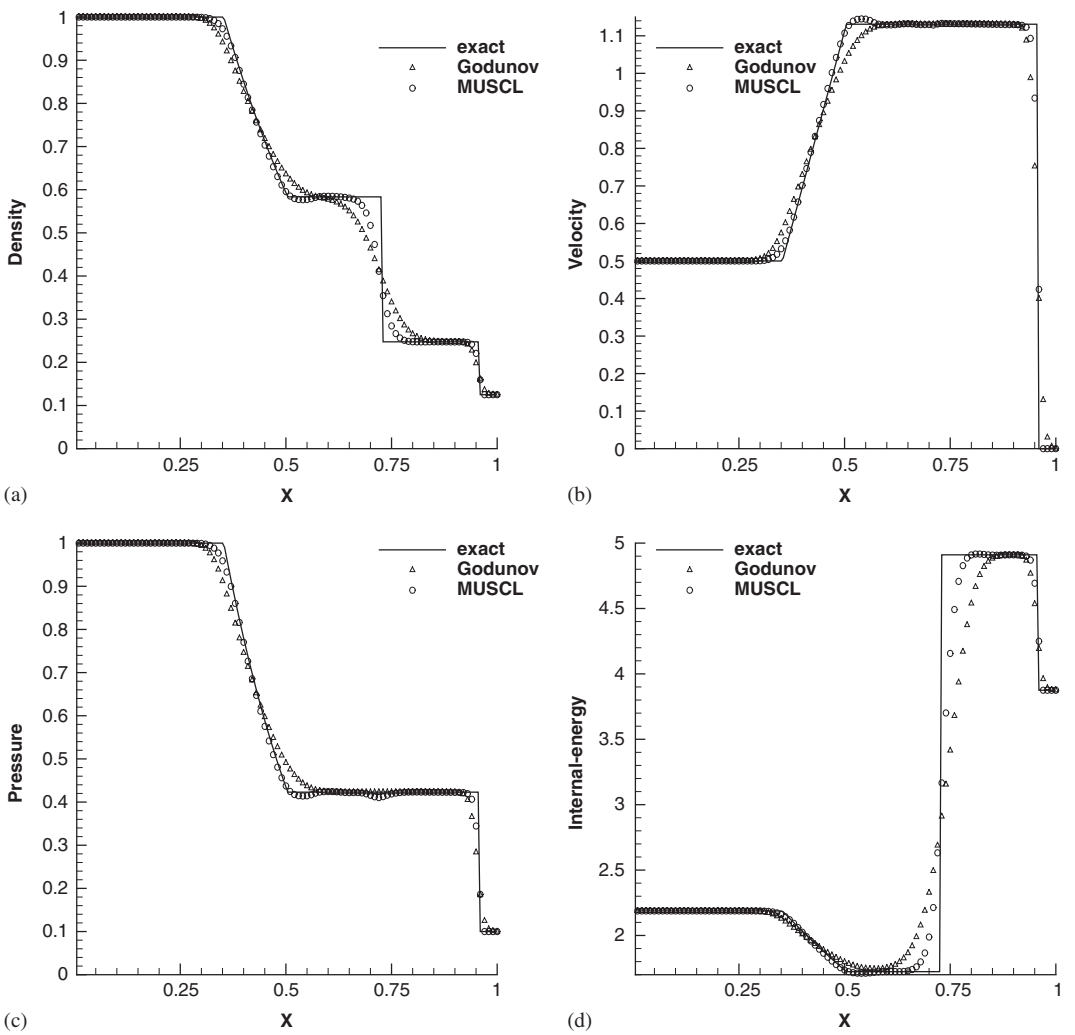

Figure 15. Test 4.3 Godunov scheme and MUSCL scheme with the new solver (100 grids, $t = 0.01$) and the initial discontinuous point is 0.5: (a) density; (b) velocity; (c) pressure; and (d) internal-energy.

results confirm the good behavior of the new two-step splitting Riemann solver in Godunov-type methods and we believe that the solver will do well with other complex EOS.

5. EXTENSION TO TWO-DIMENSIONAL SYSTEM

Euler equations in fluid dynamics in two dimensions can be written as follows:

$$\frac{\partial U}{\partial t} + \frac{\partial F(U)}{\partial x} + \frac{\partial G(U)}{\partial y} = 0 \tag{24}$$

Copyright © 2007 John Wiley & Sons, Ltd.

DOI: 10.1002/fld

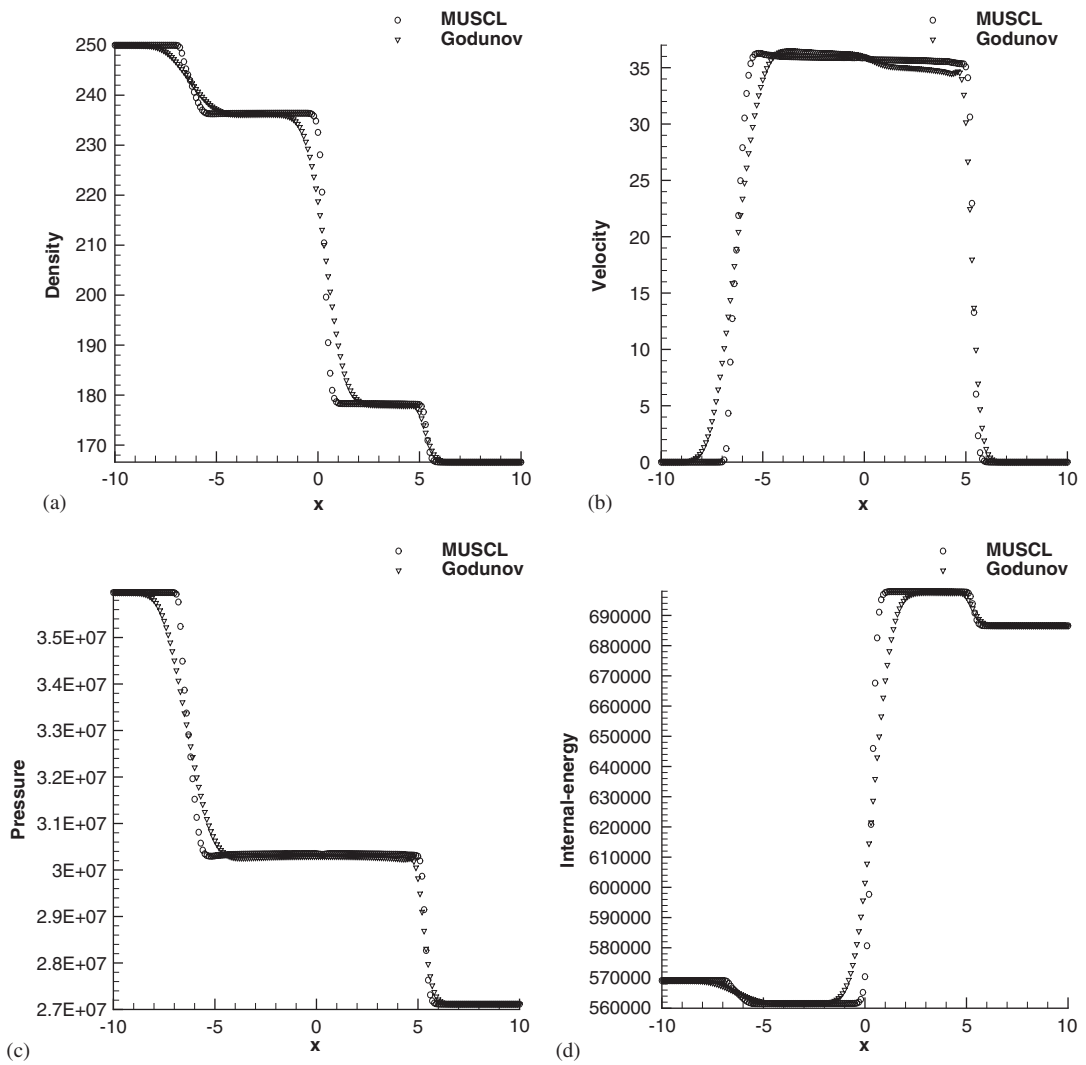

Figure 16. Test 4.4 Godunov scheme and MUSCL scheme with the new solver (200 grids, $t = 0.01$) and the initial discontinuous point is 0.0: (a) density; (b) velocity; (c) pressure; and (d) internal-energy.

with

$$U = \begin{bmatrix} \rho \\ \rho u \\ \rho v \\ E \end{bmatrix}, \quad F(U) = \begin{bmatrix} \rho u \\ \rho u^2 + p \\ \rho uv \\ u(E+p) \end{bmatrix}, \quad G(U) = \begin{bmatrix} \rho v \\ \rho uv \\ \rho v^2 + p \\ v(E+p) \end{bmatrix}$$

Copyright © 2007 John Wiley & Sons, Ltd.

DOI: 10.1002/fld

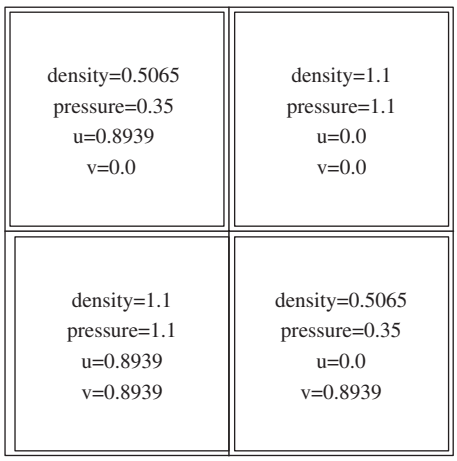

Figure 17. Initial data.

where u is the velocity in the x-direction and v is the velocity in the y-direction, $E = \frac{1}{2}\rho(u^2 + v^2) + \rho e$. Here, we only talk about the ideal gas, other gases with convex EOS can be simulated in a similar manner. Two classical methods of solving (24) are presented: the first approach is dimensional splitting or method of fractional step [24, 25]. In this approach, one applies 1-D methods to solve the 1-D Euler equations augmented by the extra component of velocity present in 2-D systems. The other approach is the finite volume method, whereby in updating the solution within some control volume one includes all the intercell flux contributions in a single time step.

Here, we find the Jacobian matrix of the x-split equations and y-split equations, $A(U) = \partial F/\partial U$, $B(U) = \partial G/\partial U$. The eigenvalues of A are as follows:

$$\lambda_1 = u - a, \quad \lambda_2 = \lambda_3 = u, \quad \lambda_4 = u + a$$

Like the method in Section 2, we can select the approximations of $\lambda_1 = u - a$, $\lambda_4 = u + a$ and then have the value of W_x. Similarly, W_y can be given. System (24) can be rewritten as follows:

$$\frac{\partial U}{\partial t} + \frac{\partial F_1(U)}{\partial x} + \frac{\partial F_2(U)}{\partial x} + \frac{\partial G_1(U)}{\partial y} + \frac{\partial G_2(U)}{\partial y} = 0 \tag{25}$$

where

$$\begin{aligned} F_1(U) &= F(U) + W_x U, \quad F_2(U) = -W_x U \\ G_1(U) &= G(U) + W_y U, \quad G_2(U) = -W_y U \end{aligned} \tag{26}$$

In a dimensional splitting method, one can use the algorithm in Section 2.3 to simulate 2-D problems without any difficulties. In a finite volume method and on non-distorted meshes, the new solver can be also applied easily.

Let us consider two particular instances of the RPs in two dimensions described in [26] and these problems have been used as test cases for numerical simulations in [27, 28]. Here, we consider the classical compressible Euler equations for an ideal gas. In the RPs for 2-D gas dynamics, the

Copyright © 2007 John Wiley & Sons, Ltd.

DOI: 10.1002/fld

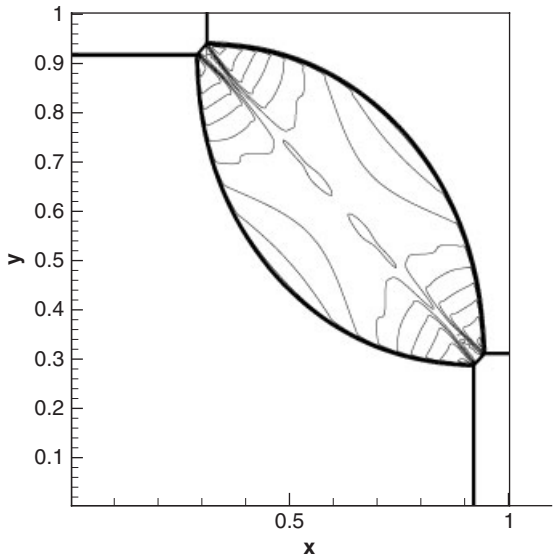

Figure 18. MUSCL scheme (400×400 grids).

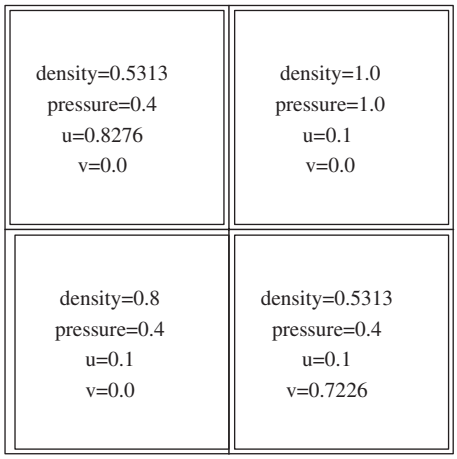

Figure 19. Initial data.

initial data are constants in each quadrant and so restricted that only one elementary wave, a 1-D shock, a 1-D rarefaction wave or a 2-D slip line appears in each interface. To simulate the RPs in 2-D Euler equations, the resolution and dissipation are both important. High resolution is needed and moderate dissipation is helpful to restrain oscillations and some instabilities. In the two tests, we show that the MUSCL scheme with the new solver is perfect by dimensional splitting method. In the calculation, we have used 400×400 grids with the CFL number equal to 0.8.

Copyright © 2007 John Wiley & Sons, Ltd.

DOI: 10.1002/fld

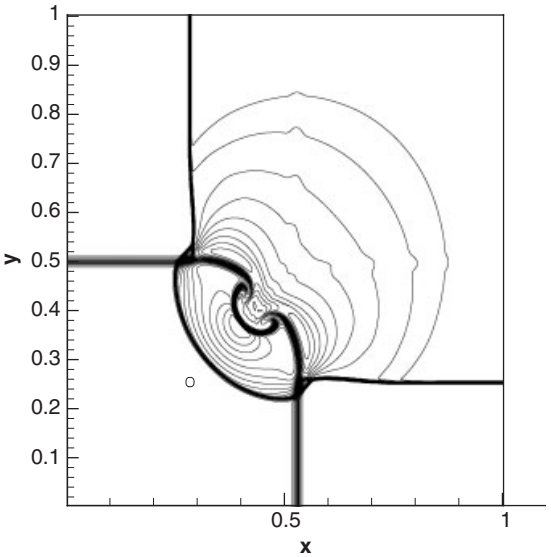

Figure 20. MUSCL scheme (400×400 grids).

5.1. *Test 5.1*

This is a four-shock situation. Its initial conditions are given in Figure 17. The numerical result at $t = 0.25$ is given in Figure 18 in the density contour lines. The resolution of our method is competitive with that in [27, 28]. But our result is more symmetric and is less oscillatory than that in [27, 28]. This is due to a moderate dissipation in our method.

5.2. *Test 5.2*

This situation has two slip lines and two rarefaction waves. The initial conditions of this test at $t = 0.3$ are given in Figure 19. The numerical result is shown in Figure 20 in the density contour lines. The figure is close to those in [27, 28], but there are no oscillations in our result compared to that in [28].

6. CONCLUSION

Godunov-type methods are characterized by the use of an RP solution to resolve discontinuities at the interface between cells. The main block of this method is the difficulty and the high cost of solving the non-linear RP exactly, especially for materials with complex EOS. This paper presents a new simple Riemann solver for Godunov-type schemes for the Euler equations. This method is less dependent on the EOS. In the numerical tests, the new Riemann solver shows its popularity in many complex EOS and good comparison with an exact Riemann solver.

Moreover, a robust study has been presented in an ideal gas. The practical behavior of the new solver when computing sonic rarefaction wave, strong shock wave, slow shock wave, etc. has been investigated. All schemes perform well in all experiments. The main drawback of the new

Copyright © 2007 John Wiley & Sons, Ltd.

DOI: 10.1002/fld

solver comparing with an exact solver is that the scheme has more dissipation that is obviously introduced by a two-step splitting method. Hence, the accuracy in a first-order Godunov scheme is less than that of an exact Riemann solver. However, when combined with high-order Godunov-type schemes, i.e. the MUSCL scheme and WENO scheme, it shows high accuracy. We believe that if more high-order reconstruction techniques, which are based upon the slope limiters (such as PPM, ENO) are taken into account, the two-step splitting Riemann solver can work efficiently with high accuracy. In 2-D cases, the new solver shows some good results which preserve high resolution and have moderate dissipation to restrain oscillations.

The framework of this paper has been restricted to the computation by finite volume methods of the Euler equations in one-space dimension and two-space dimensions. Finally, this approach can be generalized and applied to solve other systems of partial differential equations that can be expressed as hyperbolic conservation laws.

ACKNOWLEDGEMENTS

We thank the two reviewers for their numerous constructive comments and suggestions that helped improving the paper significantly. We also thank the editor for editorial revisions to our article. This work is supported in part by the National Natural Science Foundation of China under Grant No. 10431050 and CAEP under Grant No. 2003Z0603, LCP under Grant No. 51479020105ZW0902.

REFERENCES

1. Godunov SK. A finite difference method for computation of discontinuous solutions of the equations of fluid dynamics. *Matematicheskii Sbornik* 1959; **47**:271–306.
2. Einfeldt B. On Godunov-type methods for gas dynamics. *SIAM Journal on Numerical Analysis* 1988; **25**:29–318.
3. Toro EF. *Riemann Solver and Numerical Methods for Fluid Dynamics* (2nd edn). Springer: Berlin, 1999.
4. Roe PL. Approximate Riemann solvers, parameter vector and difference schemes. *Journal of Computational Physics* 1981; **43**:357–372.
5. Roe PL, Pike J. *Efficient Construction and Utilisation of Approximate Riemann Solutions*. Computing Methods in Applied Science and Engineering. North-Holland: Amsterdam, 1984.
6. Harten A, Lax PD, van Leer B. On upstream differencing and Godunov-type schemes for hyperbolic conservation laws. *SIAM Review* 1983; **25**:35–61.
7. Toro EF, Spruce M, Speares W. Restoration of the contact surface in the HLL-Riemann solver. *Shock Waves* 1994; **4**:25–34.
8. Buffard T, Gallouët T, Hérard JM. A sequel to a rough Godunov scheme: application to real gases. *Computers & Fluids* 2000; **29**:813–847.
9. Gallouët T, Hérard JM, Seguin N. Some recent finite volume schemes to compute Euler equations using real gas EOS. *International Journal for Numerical Methods in Fluids* 2002; **39**:1073–1138.
10. Lax PD. Weak solutions of nonlinear hyperbolic equations and their numerical computation. *Communications on Pure and Applied Mathematics* 1954; **7**:159–193.
11. Lax PD, Wendroff B. System of conservation laws. *Communications on Pure and Applied Mathematics* 1960; **13**:217–237.
12. Menikoff R, Plohr B. The Riemann problem for fluid flow of real materials. *Reviews of Modern Physics* 1989; **61**:75–129.
13. Van Leer B. Towards the ultimate conservative difference scheme II. Monotonicity and conservation combined in a second order scheme. *Journal of Computational Physics* 1974; **14**:361–370.
14. Van Leer B. Towards the ultimate conservative difference scheme V. A second order sequel to Godunov's method. *Journal of Computational Physics* 1979; **32**:101–136.
15. Colella P, Woodward PR. The piecewise parabolic method (PPM) for gas-dynamical simulations. *Journal of Computational Physics* 1984; **54**:174–201.
16. Liu XD, Osher S. Convex ENO high order multi-dimensional schemes without field by field decomposition or staggered grids. *Journal of Computational Physics* 1998; **142**:304–338.

Copyright © 2007 John Wiley & Sons, Ltd.

DOI: 10.1002/fld

17. Harten A, Engquist B, Osher S, Chakravathy R. Uniformly high order accurate essentially ono-oscillatory schemes III. *Journal of Computational Physics* 1987; **71**:231–303.
18. Sod GA. A survey of several finite difference methods for systems of nonlinear hyperbolic conservation laws. *Journal of Computational Physics* 1978; **27**:1–31.
19. Woodward P, Colella P. The numerical simulation of two-dimensional fluid flow with strong shocks. *Journal of Computational Physics* 1984; **54**:115–173.
20. Roberts TW. The behavior of flux difference splitting schemes near slowly moving shock waves. *Journal of Computational Physics* 1990; **10**:141–160.
21. Ivings MJ, Causon DM, Toro EF. On Riemann solvers for compressible liquids. *International Journal for Numerical Methods in Fluids* 1998; **28**:392–418.
22. Jackson Jr JE, Jamnia MA. Non-linear FSI due to underwater explosions. *Journal of Engineering Mechanics* 1984; **110**:507–517.
23. Shyue KM. A fluid-mixture type algorithm for compressible multicomponent flow with van der Waals equation of state. *Journal of Computational Physics* 1999; **156**:43–88.
24. Strang G. On the construction and comparison of difference schemes. *SIAM Journal on Numerical Analysis* 1968; **5**:506–517.
25. Yanenko NN. *The Method of Fractional Steps*. Springer: New York, 1971.
26. Schulz-Rinne CW. Classification of the Riemann problem for two-dimensional gas dynamics. *SIAM Journal on Mathematical Analysis* 1993; **24**:76–88.
27. Schulz-Rinne CW, Collins JP, Glaz HM. Numerical solution of the Riemann problem for two-dimensional gas dynamics. *SIAM Journal on Scientific Computing* 1993; **14**:1394–1414.
28. Lax PD, Liu X-D. Solution of the Riemann problem of two-dimensional gas dynamics by positive schemes. *SIAM Journal on Scientific Computing* 1998; **19**:319–340.

Copyright © 2007 John Wiley & Sons, Ltd.

DOI: 10.1002/fld